Acta Biomaterialia 10 (2014) 1940–1954

Contents lists available at ScienceDirect

Acta Biomaterialia

journal homepage: www.elsevier.com/locate/actabiomat

Immobilization of heparin/poly-L-lysine nanoparticles on dopamine-coated surface to create a heparin density gradient for selective direction of platelet and vascular cells behavior

Tao Liu [a], Yang Liu [a], Yuan Chen [a], Shihui Liu [a,b], Manfred F. Maitz [a,c], Xue Wang [a], Kun Zhang [a], Jian Wang [a], Yuan Wang [a], Junying Chen [a,*], Nan Huang [a]

[a] Key Laboratory of Advanced Technology of Materials, Ministry of Education, Southwest Jiaotong University, Chengdu 610031, People's Republic of China
[b] Naton Medical Group, Peking 100082, People's Republic of China
[c] Leibniz Institute of Polymer Research Dresden, Max Bergmann Center of Biomaterials, Hohe Str. 06, 01069 Dresden, Germany

ARTICLE INFO

Article history:
Received 9 September 2013
Received in revised form 22 November 2013
Accepted 9 December 2013
Available online 14 December 2013

Keywords:
Heparin
Nanoparticle
Endothelial cell
Blood compatibility
Intimal hyperplasia

ABSTRACT

Restenosis, thrombosis formation and delayed endothelium regeneration continue to be problematic for coronary artery stent therapy. To improve the hemocompatibility of the cardiovascular implants and selectively direct vascular cell behavior, a novel kind of heparin/poly-L-lysine (Hep/PLL) nanoparticle was developed and immobilized on a dopamine-coated surface. The stability and structural characteristics of the nanoparticles changed with the Hep:PLL concentration ratio. A Hep density gradient was created on a surface by immobilizing nanoparticles with various Hep:PLL ratios on a dopamine-coated surface. Antithrombin III binding quantity was significantly enhanced, and in plasma the APTT and TT times as coagulation tests were prolonged, depending on the Hep density. A low Hep density is sufficient to prevent platelet adhesion and activation. The sensitivity of vascular cells to the Hep density is very different: high Hep density inhibits the growth of all vascular cells, while low Hep density could selectively inhibit smooth muscle cell hyperplasia but promote endothelial progenitor cells and endothelial cell proliferation. These observations provide important guidance for modification of surface heparinization. We suggest that this method will provide a potential means to construct a suitable platform on a stent surface for selective direction of vascular cell behavior with low side effects.

1. Introduction

Cardiovascular disease (CVD) is a leading cause of mortality. Percutaneous coronary intervention using metal stents has become an important therapy for vascular stenosis in CVD. However, due to the lack biocompatibility of stent metal as well as vascular endothelium injury caused by stent implantation, postoperative vascular thrombosis, inflammation and restenosis remain problematic. The use of drug-eluting stents (DESs) loaded with anti-proliferative drugs has shown significant effect in suppressing smooth muscle cell (SMC) proliferation and contributes to a 50–70% reduction in in-stent restenosis and target lesion revascularization compared to bare metal stents [1]. However, side effects such as delayed endothelium healing remain and may trigger late restenosis and thrombosis formation. In addition, toxic polymer degradation products and exposure of the polymer coating after drug elution also tend to cause inflammation, thrombosis and intimal hyperplasia [2]. Less application of polymers, selective inhibition of thrombosis formation or intimal hyperplasia, and accelerated endothelialization seem necessary to satisfy the requirements of clinical therapy.

Heparin is clinically the most commonly used anticoagulant drug and has also been widely used as an anticoagulant coating of blood-contacting material surfaces [3–5]. The anticoagulation property of heparin (Hep) depends on its specific interaction with antithrombin III (AT III), which causes a rapid inactivation of thrombin and other proteases involved in blood clotting [6]. Numerous studies have also shown that Hep can inhibit migration and proliferation of blood vessel cells, especially SMCs [7–9]. This result from in vitro studies was further verified in animal testing and in clinical trials, demonstrating that a Hep-coated stent surface helps to prevent thrombosis and intimal hyperplasia [10,11]. In addition, early in the 1960s, Hep was shown to exhibit excellent performance as an anti-inflammatory drug in various models of inflammatory disease [12,13]. The multifunctional properties of Hep are generally attributed to its interactions with various proteins; to date, more than 100 Hep-binding proteins have been identified [14]. In different experimental setups, Hep may exhibit different or even opposite functions in directing cell behavior.

* Corresponding author. Tel.: +86 28 87634148; fax: +86 28 87600625.
E-mail address: chenjy@263.net (J. Chen).

1742-7061/$ - see front matter © 2014 Acta Materialia Inc. Published by Elsevier Ltd. All rights reserved.
http://dx.doi.org/10.1016/j.actbio.2013.12.013

For example, Yu et al. [15] demonstrated that stromal cell-derived factor-1α (SDF-1α)-immobilized Hep coating promotes the recruitment of endothelial progenitor cells and SMCs, though the antiproliferant effect of Hep is apparently blocked after binding with the cytokine. Moreover, Hep is always considered to harm endothelial cells (ECs) [16,17]; however, our recent studies suggested that an appropriate Hep dosage selectively enhances EC but inhibits SMC proliferation [18]. This means that a heparinized surface with adequate drug density and release kinetics will inhibit thrombosis and restenosis but will not harm the endothelium. Sakiyama-Elbert [19] provided a relatively comprehensive overview of the incorporation of Hep into biomaterials. The most commonly used methods to conjugate Hep seem to be covalent immobilization or electrostatic binding [20–22]. The former is considered to be stable, but protein binding and anticoagulant activity are reduced due to the use of bioactive carboxylic groups for the immobilization chemistry and the reduced steric accessibility of the immobilized molecule [23,24]. Electrostatic binding does no harm to Hep bioactivity, though burst release remains a major limitation due to the insufficient binding force. In addition, it still appears difficult to control the Hep binding density on a surface.

In this study, a Hep density gradient is constructed on a polydopamine-coated material surface with high stability and bioactivity, and the influence of different Hep densities is probed with respect to the behavior of platelets, plasma proteins, as well as vascular cells including endothelial progenitor cells (EPCs), ECs and SMCs. Polydopamine is a mussel-inspired adhesive coating, which has become attractive in the biomaterials field due to its ability to form strong adhesive interactions with materials [25,26] and with functional biomolecules that contain amine groups [27,28]. However, Hep is a highly sulfated glycosaminoglycan, rich in hydroxyl, carboxyl and sulfo groups but almost free of amine groups, and hence does not directly bind to a dopamine-coated surface.

In this study, a novel Hep immobilizing approach is introduced by covalently binding Hep/poly-L-lysine (PLL) nanoparticles onto dopamine-coated surface. A similar method has been adopted by Park et al. [29], though the protocol of nanoparticle preparation and the experimental system they used are very different from our work. As a cationic polymer of amino acids, PLL is commonly used for loading of negatively charged biomolecules, e.g. as gene vectors. Nevertheless, PLL shows a low level of transfection efficiency due to the tight interactions between PLL/DNA complexes [30]. The drawback of PLL in gene transfer, however, could constitute an advantage in terms of immobilizing biomolecules on surfaces. In the present study, amine-rich PLL is mixed with negatively charged Hep to construct Hep/PLL nanoparticles. Nanoparticles with different Hep:PLL concentration ratios are subsequently immobilized onto dopamine (DM)-coated surfaces; the change in the exposed amine group on different nanoparticles directly influences the total amount immobilizes and thereby creates a Hep density gradient surface. Taking the influence of exposed amine groups into consideration, we have demonstrated that the behavior of platelets, EPCs, ECs and SMCs can be selectively regulated over a certain Hep density range.

2. Materials and methods

2.1. Materials and reagents

316L stainless steel coupons (316L SS, Φ10 mm diameter) were mirror-polished and ultrasonically cleaned twice with acetone, absolute alcohol and reverse osmosis (RO) water in sequence for 5 min each time before use. DM, PLL (MW 150,000–300,000), Toluidine Blue O (TBO), Acid Orange II (AO II), rhodamine and 4′,6-diamidino-2-phenylindole (DAPI) were purchased from Sigma–Aldrich. Low molecular weight Hep (MW < 8000, potency > 160 U mg^{-1}) was purchased from Shanghai Bio Science & Technology Company. Rabbit monoclonal anti mouse CD34 antibody, rabbit monoclonal anti-human α-SMA antibody, fluorescein isothiocyanate (FITC)-conjugated goat anti-rabbit IgG antibody and FITC-conjugated goat anti-mouse IgG antibody were purchased from Boster Biological Technology (Wuhan, PR China), rabbit monoclonal anti-human vWF antibody and mouse monoclonal anti-human p-selectin antibody were purchased from Sigma–Aldrich. Mouse monoclonal anti-human AT III antibody, horseradish peroxidase (HRP)-conjugated goat anti-mouse IgG antibody and TMB (3,3′,5,5′-tetramethylbenzidene) color developing agent were purchased from BD Bioscience (San Jose, CA). Mouse monoclonal anti-human fibrinogen (FGN) γ chain antibody was purchased from Abcam (UK). 0.01 M phosphate-buffered saline (PBS, pH 7.4) was used for PLL and Hep solution preparation.

2.2. Hep/PLL nanoparticle preparation and immobilization

A schematic diagram of Hep/PLL nanoparticle preparation and immobilization is shown in Fig. 1. First, different concentrations of Hep solution were added to 0.5 mg ml^{-1} PLL solution with equal volumes under ultrasonic condition for 5 min to create a range of Hep/PLL nanoparticles; detailed parameters and the Hep/PLL nanoparticle names are listed in Table 1. For DM coating preparation, 316L SS samples were immersed into 2 mg ml^{-1} DM solution (dissolved in 10 mM Tris buffer, pH 8.5) at 20 °C for 12 h, after which the samples were ultrasonically washed three times with ultra-pure (UP) water for 5 min each and marked as layer 1. The above operation was repeated twice more, so a total of three layers of DM was grafted on to the sample surfaces. Subsequently, the DM-coated 316L SS samples were immersed into different Hep/PLL nanoparticle solutions and incubated at 20 °C for 12 h with gentle shaking, and then finally washed three times with PBS and UP water for 5 min to construct Hep/PLL nanoparticle-immobilized samples.

2.3. Nanoparticle size and zeta potential analysis

The mean size and particle dispersion index (PDI), as well as the zeta potential of the Hep/PLL nanoparticles dispersed in PBS medium were determined by dynamic light scattering (DLS) using a Zetasizer Nano-ZS90 (Malvern Ltd., Malvern, UK). Each measurement was repeated three times.

2.4. FTIR

The changes of surface chemical group composition after Hep/PLL nanoparticle immobilization was determined by Fourier transform infrared spectroscopy (FTIR) (Nicolet 5700 infrared spectrometer, USA) using the model of diffuse reflectance. Scanning was conducted in the range from 400 to 4000 cm^{-1}.

2.5. XPS

The surface chemical elemental composition of DM-coated and Hep/PLL nanoparticle-immobilized samples was investigated by X-ray photoelectron spectroscopy (XPS) (Kratos Ltd., UK) on an AXIS His spectrometer with a monochromatic Al K_α X-ray source (1486.6 eV photons, 150 W); the pressure in the chamber was $<2 \times 10^{-9}$ Torr. The binding energy scale was referenced by setting the C_{1s} peak at 284.6 eV.

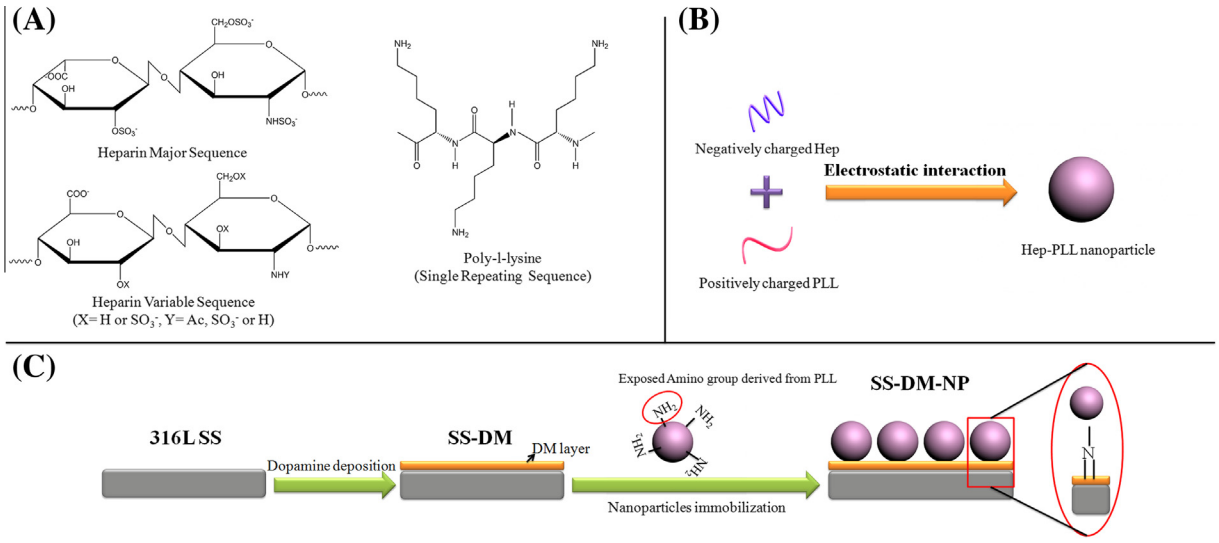

Fig. 1. Schematic drawing of the immobilization method of Hep/PLL nanoparticles on the dopamine-coated surface. (A) Chemical structure of Hep and PLL; (B) Hep/PLL nanoparticle preparation; (C) Hep/PLL nanoparticle immobilization process.

Table 1
Composition of the nanoparticles.

Nanoparticle ID	Preparation of the nanoparticles
NP0.5	0.5 mg ml^{-1} PLL mixed with equal volume 0.5 mg ml^{-1} Hep
NP1.0	0.5 mg ml^{-1} PLL mixed with equal volume 1.0 mg ml^{-1} Hep
NP3.0	0.5 mg ml^{-1} PLL mixed with equal volume 3.0 mg ml^{-1} Hep
NP5.0	0.5 mg ml^{-1} PLL mixed with equal volume 5.0 mg ml^{-1} Hep
NP7.0	0.5 mg ml^{-1} PLL mixed with equal volume 7.0 mg ml^{-1} Hep
NP10.0	0.5 mg ml^{-1} PLL mixed with equal volume 10.0 mg ml^{-1} Hep

2.6. AFM

The changes in surface topography before and after Hep/PLL nanoparticle immobilization were characterized by atom force microscopy (AFM) (Nanowizard II, JPK Instruments, Berlin, Germany) in contact mode. AFM was performed at room temperature and the image analysis was processed by CSPM Imager software.

2.7. Water contact angle

Static water contact angle on samples were measured using a DSA100 Mk 2 goniometer (Krüss GmbH, Germany) at room temperature. A droplet of UP water was added to dried sample surfaces, and then the contact angle was calculated by a circle segment function of the DSA 1.8 software. There were four parallel samples in each group, and for each sample, measurements were taken at at least three different sites.

2.8. Heparin density and quantitative release characterization–TBO assay

The surface density of Hep after Hep/PLL nanoparticle immobilization was characterized by TBO assay [31]. In detail, 0.04 wt.% TBO solution was prepared by dissolving the TBO powder in aqueous 0.01 M HCl/0.2 wt.% NaCl, and then the samples were incubated in 5 ml TBO solution under static conditions at 37 °C for 4 h and rinsed three times with UP water. Subsequently, the Hep–TBO complex that formed on sample surface was eluted and dissolved in 5 ml 80% ethanol/0.1 M NaOH mixture (4/1 v/v) solution. Ultimately 150 μl of the supernatant was transferred to a 96-well plate and the absorbance was measured at 530 nm by a microplate reader (μQuant, Bio-tek Instruments Inc.), and the Hep density on the sample surface was evaluated using a calibration standard curve. There were six parallel samples in each group, and SS-DM was set as blank control.

For standard curve preparation, 2 ml 0.04 wt.% TBO was first added to 2 ml of a known concentration Hep solution and incubated at 37 °C with gentle shaking for 4 h, the Hep–TBO complex spontaneously formed and precipitated in the mixture. Then the mixture was centrifuged at 3500 rpm for 10 min, the supernatant was removed and the precipitate was carefully rinsed twice with aqueous 0.01 M HCl/0.2 wt.% NaCl. Finally, 5 ml 80% ethanol/0.1 M NaOH mixture (4/1 v/v) solution was added to dissolve the precipitate and the absorbance was measured at 530 nm.

For quantitative characterization of the Hep release, the samples were immersed in PBS at 37 °C and shaken (60 rpm) for 1, 3, 5, 7, 10, 14, 21 and 28 days in an airtight centrifuge tube. The release medium at each time point was collected and the amount of Hep released was measured by using the same procedure based on a standard curve preparation. There were six parallel samples in each group, and the density of the residual Hep on the sample surfaces at each time point was measured by TBO assay as described above.

2.9. Amine density quantitative characterization–AO II test

The Acid Orange II (AO II) test was used here to determine the surface amine density after Hep/PLL nanoparticle immobilization [32]. In detail, 0.5 mM AO II solution was prepared by dissolving 8.75 mg AO II powder in 50 ml HCl (pH 3) solution. Then the samples were incubated in 1 ml of AO II solution with gentle shaking at 37 °C for 6 h; subsequently samples were rinsed thee times with pH 3 HCl for 5 min each. The samples were then immersed into 1 ml NaOH solution dissolved in UP water, pH 10, and shaken for 15 min at 37 °C to dissolve the absorbed AO II on the sample surfaces. Ultimately, 150 μl of supernatant was transferred to a 96-well plate and the absorbance of the supernatant was determined in a microplate reader at 485 nm; the amine density on the sample surfaces was evaluated by a standard calibration curve. There were six parallel samples in each group, and 316L SS was set as blank control (data not shown).

For standard curve preparation, 0.5 mM AO II solution in 10 mM NaOH was prepared and serial twofold dilutions with 10 mM NaOH were made; the absorbance of the known concentration AO II solutions was then measured in a microplate reader at 485 nm.

2.10. Blood compatibility evaluation

Fresh human whole blood used in blood compatibility evaluation was obtained lawfully from Chengdu Blood Center, PR China. The experiment was performed within 12 h after the blood donation and the blood was anticoagulated with 3.8% sodium citrate in a volume ratio of 1:9 ($V_{citrate}$:V_{blood}). There were six parallel samples for microscopy observation or clotting time assay and eight parallel samples for immunochemistry assay. 316L SS and SS-DM were used as positive control.

2.10.1. Platelet adhesion and LDH assay

An in vitro platelet adhesion test was used to evaluate the surface thrombogenicity of the samples. Fresh human whole blood was first centrifuged at 1500 rpm for 15 min to obtain platelet-rich plasma (PRP). Then, 50 μl PRP was added to the sample surface and incubated at 37 °C for 1 h. Subsequently, the samples were rinsed three times with PBS for 3 min each and used for morphology observation and lactate dehydrogenase (LDH) assay.

For platelet morphology observation, the above samples were fixed in 2.5% glutaraldehyde for 12 h at room temperature and then dehydrated and dealcoholized; after critical point drying with CO_2, the samples were coated with a gold layer and observed by scanning electron microscopy (SEM; Philips Quanta 200).

LDH assay was used to quantify the amount of platelets adhered on the sample surfaces. In detail, 50 μl of 1% Triton X-100 was added to the sample surfaces and incubated at 37 °C for 5 min, and then 25 μl of lysate was taken from the surfaces and mixed with 200 μl Tris(hydroxymethyl)aminomethane base buffer mixture containing 0.28 mg ml^{-1} nicotinamide adenine dinucleotide reduced (NADH) and 0.187 mg ml^{-1} pyruvate in a 96-well plate. Finally, the absorbance was measured in a microplate reader at 340 nm. The LDH activation of adherent platelets on the sample surfaces was calibrated using a calibration curve of a defined concentration of lysed platelets.

2.10.2. Platelet activation and p-selectin assay

P-Selectin expression was determined as marker of platelet activation induced by the surfaces. Firstly, 50 μl PRP was added to the sample surfaces and incubated at 37 °C for 1 h. Then the samples were rinsed three times with PBS, and used for p-selectin immunofluorescence staining and semiquantitative chara cterization.

For p-selectin immunofluorescence staining, the above samples were fixed in 4% paraformaldehyde for 12 h at room temperature and rinsed three times with PBS for 3 min each; the samples were then incubated in goat serum (1:10 in PBS) at 37 °C for 1 h to block nonspecific adsorption. Subsequently 30 μl mouse monoclonal anti-human p-selectin antibody (first antibody, 1:200 in PBS) was added to surfaces at 37 °C for 1 h and washed three times with PBS for 3 min each; after that 30 μl FITC-conjugated goat anti -mouse IgG antibody (second antibody, 1:100 in PBS) was added to surfaces and incubated at 37 °C for 30 min and washed three times with PBS for 3 min each. Finally, the samples were observed by fluorescence microscopy (Olympus IX51, Japan).

For semiquantitative characterization of p-selectin, the procedure of PRP and first antibody incubation was the same as immunofluorescence staining. Horseradish peroxidase (HRP)-conjugated goat anti-mouse IgG antibody was used as the second antibody and incubated at 37 °C for 30 min. After rinsing three times with PBS, 100 μl TMB agent was added to the sample surface and reacted for 10 min. The color reaction was stopped by adding 50 μl of 1 M H_2SO_4 and 100 μl of the reaction solution was transferred to a 96-well plate; the absorbance was then measured at 450 nm.

2.10.3. AT III binding and fibrinogen conformation change

The amount of absorbed AT III on the sample surface was determined semiquantitatively by immunochemistry. In detail, fresh human whole blood was first centrifuged at 3000 rpm for 15 min to obtain platelet-poor plasma (PPP). Then 50 μl PPP was added to the samples and incubated at 37 °C for 15 min. After rinsing three times with PBS, the adsorbed AT III was quantified by immunochemistry as described above. The initial non-dilute concentration of HRP labeled antibody that was used to make the standard curve is taken as 100%.

The conformation change of absorbed fibrinogen on the sample surface was investigated after PPP adsorption on the sample for 1 h. The exposure of fibrinogen γ chain was detected by immunochemical quantification using the same procedure as in the AT III assay except for the difference of the first antibody. Here, the first antibody was mouse monoclonal anti-human fibrinogen γ-chain-specific antibody, which corresponded to amino acids 210–437 of the γ chain.

2.10.4. APTT, PT and TT

Activated partial thromboplastin time (APTT) and thrombin time (TT) were measured to evaluate the influence of sample surface on the coagulation system. In detail, 500 μl PPP was added to the samples and incubated at 37 °C for 30 min.

For the APTT test, 100 μl incubated PPP was transferred to the test tube, followed by addition of 100 μl APTT agent and incubated at 37 °C for 3 min; subsequently 100 μl 0.025 M $CaCl_2$ was added and the clotting time was measured in an automatic blood coagulation analyzer (ACL-200, Beckman Coulter, USA).

For PT and TT test, 100 μl PT or TT reagent was added to the test tube, followed by adding 100 μl incubated PPP and then incubating at 37 °C for 3 min; subsequently the clotting time was measured using an automatic blood coagulation analyzer.

2.11. Cellular compatibility evaluation

2.11.1. EPC, EC and SMC isolation and culture

EPCs were isolated and cultivated from the bone marrow of Sprague–Dawley (SD) rats (Sichuan University, Chengdu, PR China) and cultured according to Li et al. [33] with some modifications. Briefly, the bone marrow of SD rats was extracted and blown into suspension with α-Modified Eagle's Medium (α-MEM) containing 10% fetal bovine serum (FBS), and then the suspended cells were seeded in culture flasks and incubated at 37 °C under 5% CO_2. The medium was changed every 2 days and the cells were trypsinized for subculture at confluency. After 1 week, the cells were considered as pure bone marrow stem cells (BMSCs) and then cultured in α-MEM with 10% FBS and 10 ng ml^{-1} VEGF. After 2 weeks of culture, cells are designated as EPCs based on the identification of cell morphology and specific markers.

ECs were isolated from human umbilical vein. Briefly, a needle was inserted into the umbilical vein and the lumen washed thoroughly with physiological saline to remove the residual blood. Then 0.1% type II collagenase in medium 199 (M199) was added and incubated at 37 °C for 15 min. The digestion was stopped by filling M199 with 10% FBS. Subsequently, the suspended cells were collected by centrifugation at 1000 rpm for 8 min, and finally the supernatant was removed and the cells were resuspended in M199 with 15% FBS and 20 μg ml^{-1} endothelial cell growth supplement (ECGS, mainly aFGF and bFGF) and incubated at 37 °C under 5% CO_2.

SMCs were isolated from human umbilical artery. Briefly, the adventitia layer and endothelium layer were first stripped away from the umbilical artery. Then the residual tissue was cut into small pieces and stuck to the bottom of a culture flask. The flask was carefully inverted and to infuse 5 ml Dulbecco's Modified Eagle's Medium/F12 (DMEM/F12) with 10% FBS. The flask was subsequently incubated at 37 °C under 5% CO_2 overnight to make the tissue pieces dry up and adhere tightly to the flask. After that, the culture flask was gently inverted to allow the pieces of tissue to become fully immersed in the culture medium. SMCs were obtained by slow outgrowth from these tissue pieces. The medium was changed every 2 days and the cells were subcultured by trypsination, when confluency was reached.

2.11.2. Cell seeding on samples surface

316L SS- and DM-coated samples were sterilized by autoclaving before use, the PLL solution was prepared under aseptic conditions and the Hep solution was sterile filtered with a 0.22 μm Millipore filter, and Hep/PLL nanoparticle preparation and immobilization were carried out under aseptic conditions. EPCs, ECs and SMCs were seeded on the sample surfaces at an identical density of 5×10^4 cells ml^{-1} and incubated at 37 °C under 5% CO_2 for 1 and 3 days, respectively. α-MEM with 10% FBS was used as culture medium for EPC culture and M199 with 15% FBS and 20 μg ml^{-1} ECGS was used for EC culture. For SMCs, the culture medium was DMEM/F12 with 10% FBS.

2.11.3. Cell proliferation assay

The proliferation activity of different cells on the sample surfaces was investigated with a Cell Counting Kit-8 (CCK-8) after 3 days of culture. The medium was removed and the samples were washed twice with PBS. Then, 400 μl fresh medium that was consistent with with the EPC, EC or SMC seeding medium but containing 10% CCK-8 reagent was added to the samples and incubated at 37 °C under 5% CO_2 for an identical time of 3 h. Subsequently the absorbance was measured at 450 nm. There were eight parallel samples in each group. 316L SS and SS-DM were used as positive control and the medium containing 10% CCK-8 was used as blank control.

2.11.4. Immunofluorescence staining

Immunofluorescence staining was preformed to identify the types and observe the morphology of adherent cells on the sample surfaces by using specific antibodies. There were six parallel samples in each group for fluorescence microscopy observation. Briefly, the sample cultures with cells were washed three times with PBS after 3 days of culture and then fixed in 4% paraformaldehyde for 12 h at room temperature. After that, the samples were incubated with goat serum (1:10 in PBS) at 37 °C for 1 h to block nonspecific adsorption. Subsequently, specific antibodies (first antibody, 1:200 in PBS) were added to the sample surfaces and incubated at 37 °C for 30 min. After washing three times with PBS, FITC-conjugated goat anti-rabbit IgG antibody (second antibody, 1:100 in PBS) was added to the samples and incubated at 37 °C for 30 min. The first antibodies used for EPC, EC and SMC determination were rabbit monoclonal anti-mouse CD34 antibody, rabbit monoclonal anti-human vWF antibody and rabbit monoclonal anti-human α-SMA antibody, respectively. Finally, the samples were thoroughly rinsed three times with PBS and observed by fluorescence microscopy.

Rhodamine and DAPI fluorescence staining were used to investigate the interactions between cells and Hep/PLL nanoparticles. Briefly, the samples cultured with EPCs, ECs or SMCs were washed three times with PBS after 1 day culture and fixed in 2.5% glutaraldehyde for 12 h at room temperature. Then 30 μl DAPI (1:400 in PBS) was added to the sample surfaces and incubated at 37 °C for 5 min. After three washes with PBS, 30 μl of rhodamine (1:1000 in PBS) was added to the samples and incubated at 37 °C for 20 min. Subsequently the samples were thoroughly rinsed three times with PBS and observed by fluorescence microscopy.

2.11.5. NO release of EPCs and ECs

The NO release was detected with minor modifications as described by Yang et al. [18]. In brief, EPCs or ECs were seeded on the samples surface at a high density of 5×10^5 cells ml^{-1}. After 6 h incubation, all samples were transferred to new 24-well plates and 1 ml fresh culture medium without phenol red was added. 100 μl of culture medium was subsequently transferred to a new 96-well plate after 12 h incubation and an equal volume of Griess reagent (Sigma) was added. The mixture was incubated for 15 min at room temperature in the dark and the absorbance was measured at 540 nm. For standard curve preparation, 100 μl of a known concentration $NaNO_2$ solution was added to a 96-well plate and then an equal volume of Griess reagent was added; after 15 min incubation the absorbance of the mixture was measured at 540 nm. There were eight parallel samples in each group and the NO release level was finally normalized to the cell number.

2.12. Statistic analysis

At least three independent experiments were performed for the assay described above. The data analyzed with the software SPSS 11.5 and expressed as a mean ± standard deviation (SD). One-way ANOVA in Origin 8.0 was used to determine the statistical significance between and within groups. A probability value $P < 0.05$ was considered significant.

3. Results

3.1. Size and zeta potential of nanoparticles

The formation of Hep/PLL nanoparticles in PBS was mainly driven by the electrostatic interaction between negatively charged Hep and positively charged PLL. Here, the size and zeta potential of Hep/PLL nanoparticles were determined to investigate the influence of Hep and PLL concentration ratio on particle formation and structural characteristics. In general, the particle system was considered moderately stable when the absolute value of the zeta potential was at least 30 mV [34]. PDI was another important indicator to evaluate the size distribution of the particles, and a smaller PDI indicated a better uniformity.

According to Fig. 2A, with an increase in Hep concentration, the mean size of the Hep/PLL particles rapidly decreased from ~1200 nm to less than 300 nm and tended to balance when the Hep concentration increased to 7.0 mg ml^{-1} (NP7.0). The PDI value showed that the uniformity of Hep/PLL nanoparticles was improved with the increase in the Hep concentration and tended to balance when the Hep concentration increased to 5.0 mg ml^{-1} (NP5.0). These results indicated that an increase of the Hep concentration promoted a positive or negative charge in the molar charge ratio and enhanced the electrostatic interactions, thereby improving the compactness and uniformity and decreasing the size of the Hep/PLL nanoparticles. Furthermore, for NP0.5 and NP1.0, the absolute value of the zeta potential was less than 20 mV, which indicated insufficient stability of the formed particles and the possibility of rapid coagulation. With the increase in Hep concentration, the Hep content in the nanoparticles increased and the exposure of positively charged amino groups on particle surface decreased due to the steric hindrance effects of Hep (Fig. 2B), which thereby directly increased the absolute value of the zeta potential (Fig. 2A). The zeta potential tended

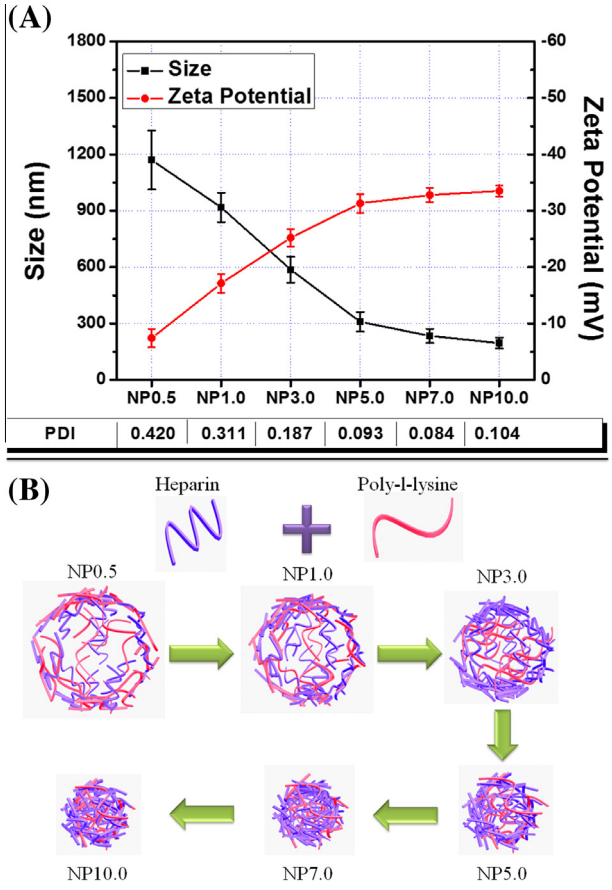

Fig. 2. (A) Sizes and zeta potential values of different nanoparticles (mean ± SD, $n = 6$). (B) The structural changes of nanoparticles with increasing heparin concentration.

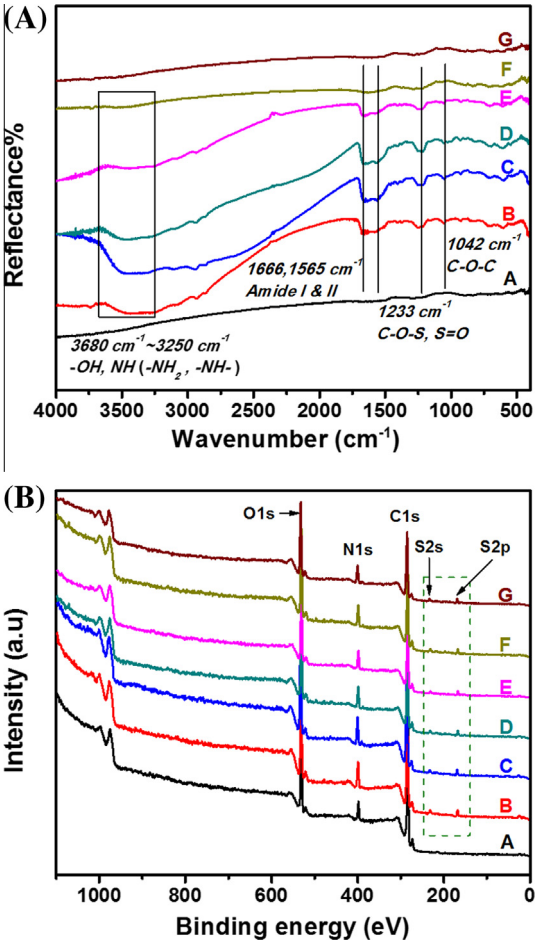

Fig. 3. Surface chemical composition characterization. (A) FTIR spectra and (B) XPS analysis of different Hep/PLL nanoparticles immobilized surfaces. A–G represent SS-DM, NP0.5, NP1.0, NP3.0, NP5.0, NP7.0 and NP10.0, respectively.

to balance when the Hep concentration reached 7.0 mg ml^{-1}, indicating that the Hep content in the nanoparticles became saturated. Some hypothesizes were further demonstrated by subsequent experiments.

3.2. FTIR and XPS

FTIR analysis was used to characterize the surface chemical group composition of DM coated with immobilized Hep/PLL nanoparticles (Fig. 3A). Compared to DM-coated 316L SS, noticeable new peaks were observed after NP0.5, NP1.0, NP3.0 and NP5.0 immobilization. A broad peak in the range from 3680 to 3300 cm^{-1} was suggested as the overlap peak of amine (–NH_2, –NH–) and hydroxyl (–OH) groups stretching vibrations; the former was considered primarily derived from PLL and the latter was from both Hep and PLL. Two new peaks at about 1666 and 1565 cm^{-1} correspond to the stretching vibrations of the amide I (C=O) and II (C–N, N–H) bonds of PLL. Characteristic Hep absorption peaks could also be observed at 1233 and 1042 cm^{-1}, and were ascribed to the S=O and C–O–C bonds, respectively. In addition, it was interesting to note that their intensity decreased with an increase in the Hep concentration. For NP7.0 and NP10.0 immobilized surfaces, no significant changes could be observed in the FTIR spectra compared with SS-DM. We speculate that the total immobilized quantity of nanoparticles decreased with the increasing Hep concentration and was below the FTIR detection limit when the Hep concentration reached 7.0 mg ml^{-1}. As proof, XPS analysis with higher detection sensitivity was used to determine the surface chemical elemental composition after nanoparticle immobilization.

The XPS wide-scan spectra of different nanoparticle-immobilized surfaces are shown in Fig. 3B. New S2s (~234.6 eV) and S2p (~168.8 eV) peaks appeared in the spectrum after nanoparticle immobilization. This means NP7.0 and NP10.0 were immobilized onto the DM-coated surface. In combination with the chemical elemental semiquantitative results (Table 2), it could be concluded that the sulfur content on the nanoparticle-immobilized surfaces dropped from 1.90% to 0.91% with an increase in the Hep concentration, which was consistent with the conclusions from FTIR. This decrease was attributed to a reduced number of exposed amine groups on the nanoparticle surface, which were necessary for grafting to the DM surface. To demonstrate this inference, further experiments were subsequently performed.

Table 2
Elemental composition of different sample surfaces determined by XPS.

Sample ID	C (%)	N (%)	O (%)	S (%)
SS-DM	77.33	6.34	16.08	0.25
NP0.5	65.79	9.86	22.53	1.82
NP1.0	65.91	9.76	22.43	1.90
NP3.0	66.47	9.22	22.74	1.57
NP5.0	67.06	8.93	22.61	1.40
NP7.0	67.33	8.17	23.45	1.05
NP10.0	68.77	8.21	22.11	0.91

3.3. Quantity of heparin and amine

The Hep density and release kinetics were investigated by TBO assay. AO II assay was used for amine group density quantification. Additional experimental had demonstrated that PLL cannot react with TBO, and that Hep also has no influence on the absorbance of AO II reagent (Fig. S1).

As shown in Fig. 4A, the Hep density on NP0.5 immobilized surface was about 30.9 ± 3.4 μg cm^{-2} and increased to 43.1 ± 5.1 μg cm^{-2} on the NP1.0 immobilized surface, which was attributed to the higher Hep level of NP1.0 compared to NP0.5. Consistent with the steric hindrance of PLL by Hep, described above, the exposed amine density decreased from 50.2 ± 2.7 nmol cm^{-2} on the NP0.5 immobilized surface to 41.2 ± 4.5 nmol cm^{-2} on the NP1.0 immobilized surface. With increasing Hep concentration, Hep continually assembled on the nanoparticles and the exposed amine density gradually decreased, which directly suppressed the reactivity of the nanoparticles with the DM layer, and thereby, although the Hep content in nanoparticles was increased, the immobilized Hep density decreased from 43.1 ± 5.1 μg cm^{-2} to 3.5 ± 0.7 μg cm^{-2} (NP10.0). These results are consistent with the FTIR and XPS result, and proved the hypothesis described in Sections 3.1 and 3.2.

According to the Hep release curves shown in Fig. 4B, there was a small burst release of Hep in all test groups within 24 h. The amount of released Hep correlated with the Hep density, for NP0.5 and NP1.0, the Hep release amounts were higher than other groups and a high release rate was maintained even after 4 weeks' immersion (Fig. 4B). However, for other groups, the release curves reached saturation after 7 days' immersion (Fig. 4B). This discrepancy may be mainly related to the difference of nanoparticle stability. Although the particle structure has a larger specific area compared with a solid film structure, the high intermolecular binding force may provide better control for sustained Hep release.

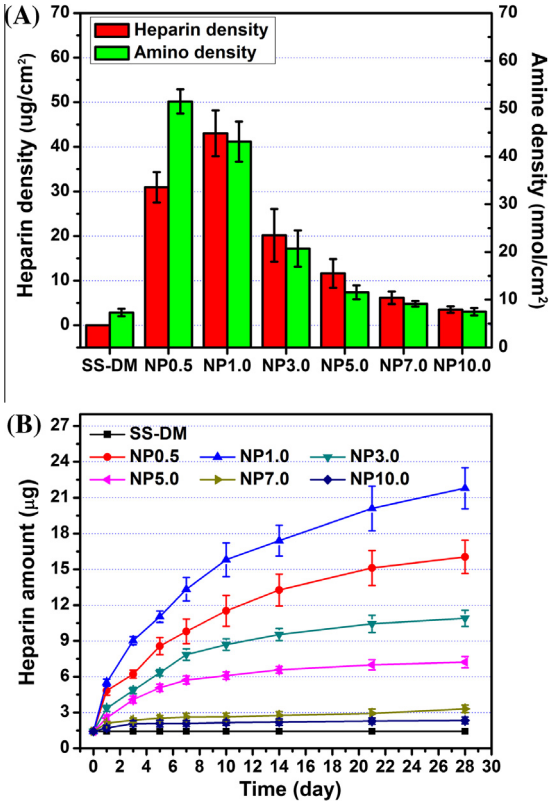

Fig. 4. (A) Quantitative characterization of the exposed heparin and amine groups on different Hep/PLL nanoparticle-immobilized surfaces by TBO assay and AO II test, respectively (mean ± SD, $n = 6$). (B) Cumulative release of heparin from different nanoparticle immobilized surfaces (mean ± SD, $n = 6$).

3.4. AFM images of nanoparticle-immobilized surface

AFM analysis was used to detect the surface topography after immobilization of different nanoparticles. Instead of showing discrete particles, NP0.5 tended to form a confluent film on the DM-coated surface (Fig. 5). With a gradual increase in the Hep concentration, for NP1.0, although significant confluence of the nanoparticles occurred, an incipient particle structure was formed on the sample surfaces (Fig. 5). A relatively uniform particle structure could be observed on the NP3.0 immobilized surface, which suggested that the nanoparticle possessed adequate stability; however, slight spreading and confluence remained. When the Hep concentration reached 5 mg ml^{-1}, the nanoparticle could be clearly observed on the surface and maintained excellent conformation after immobilization (Fig. 5). The particle density on NP7.0 and NP10.0 immobilized surface was greatly decreased compared to NP5.0, which indicating a low degree of grafting. In all, this result further proved the conclusions of the FTIR and XPS, and illustrates visually the Hep quantification.

3.5. Water contact angle

Changes in surface hydrophilicity may cause quantitative and qualitative variations of absorbed proteins, which directly influence the biocompatibility of the materials [35]. The water contact angle was measured here to evaluate the surface hydrophilicity before and after nanoparticle immobilization.

As shown in Fig. 6, the mean contact angle of 316L SS was 53.7° and this increased to 62.1° after DM deposition. The decrease in surface hydrophilicity can be explained by the exposure of hydrophobic groups such as the benzene ring of DM. Heparin and PLL are rich in hydrophilic groups, including hydroxyl, amine, carboxyl and sulfo groups. Hence, the contact angles were significantly decreased ($^*P < 0.05$) after nanoparticle immobilization (Fig. 6). Almost no variations in contact angles could be detected when the Hep concentration increased from 0.5 to 5.0 mg ml^{-1} (in the range from 25° to 30°); however, with a further increase in the Hep concentration, the contact angle slightly increased, due to the decrease in Hep and PLL density.

3.6. Blood compatibility evaluation

3.6.1. Platelet adhesion and activation

The amount and the activation profile of adherent platelets are considered as key indicators for evaluating the hemocompatibility of the surface of a material. In general, platelet morphologies were related to their activation level, with the typical shape of round, dendritic, spreading dendritic, spreading and fully spreading that corresponded to the activation stage from minor to major [28]. LDH assay was performed for semiquantitative evaluation of the number of adherent platelets. P-selectin assay was performed to further evaluate the platelet activation. In normal state, p-selectin was stored in α-granules of non-activated platelets [36]. Upon platelet activation, p-selectin bound to the membrane of the open canalicular system and was subsequently expressed on platelet membrane.

SEM images of platelet morphology (Fig. 7A) showed that large amounts of platelet aggregated on 316L SS and SS-DM sample surfaces, and the adherent platelets mainly exhibited spreading dendritic and fully spreading shape, indication significant activation and poor hemocompatibility. In contrast, the number of platelets on immobilized nanoparticles was significantly decreased (Fig. 7A), and the adherent platelets displayed a round shape,

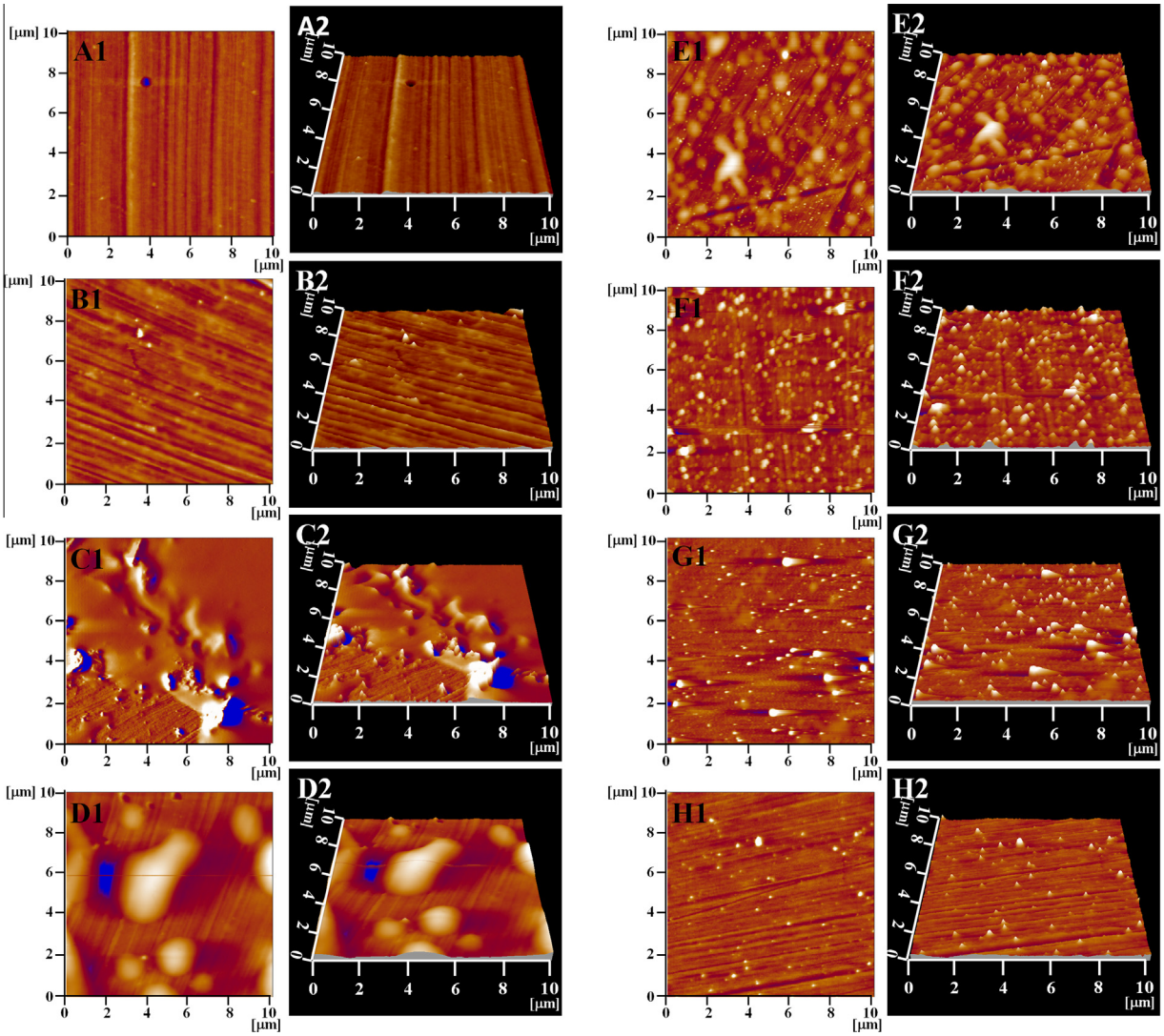

Fig. 5. AFM images of the morphology of various Hep/PLL nanoparticle-immobilized surfaces. A–H represent 316L SS, SS-DM, NP0.5, NP1.0, NP3.0, NP5.0, NP7.0 and NP10.0, respectively.

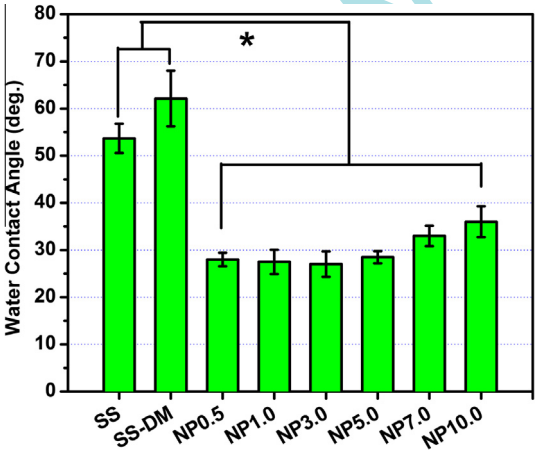

Fig. 6. Water contact angle after immobilization of various nanoparticles (mean ± SD, $n = 4$, $^*P < 0.05$ indicates significant difference compared with SS and SS-DM).

which indicated minor activation and excellent anticoagulant property. In addition, although the Hep density was very different, no obvious changes could be observed on the various nanoparticle immobilized surfaces. In agreement with the SEM result, LDH results showed that the platelet number on 316L SS and SS-DM sample surfaces was significantly higher ($^*P < 0.05$) than on the nanoparticle-immobilized surface, but there were no differences among the nanoparticle-immobilized samples (Fig. 7B).

Fig. 7C shows the p-selectin immunofluorescence staining of adherent platelets on different sample surfaces. Compared with 316L SS and SS-DM, the expression of p-selectin on the nanoparticle-immobilized surface was obviously decreased. Correspondingly, the relative quantity of expressed p-selectin was significantly reduced ($^*P < 0.05$) after nanoparticle immobilization (Fig. 7D), which further proved that the nanoparticle-modified surface could effectively inhibit platelet adhesion and activation. Similar to SEM and LDH results, the p-selectin expression level was not significantly different between the various nanoparticle-immobilized samples, which suggested that low Hep density was sufficient to achieve favorable anticoagulation.

3.6.2. AT III binding and fibrinogen conformation change

The anticoagulant property of Hep mainly depends on its interaction with AT III. The specific binding of AT III to the pentasaccharide structure of Hep triggered the conformation change, which

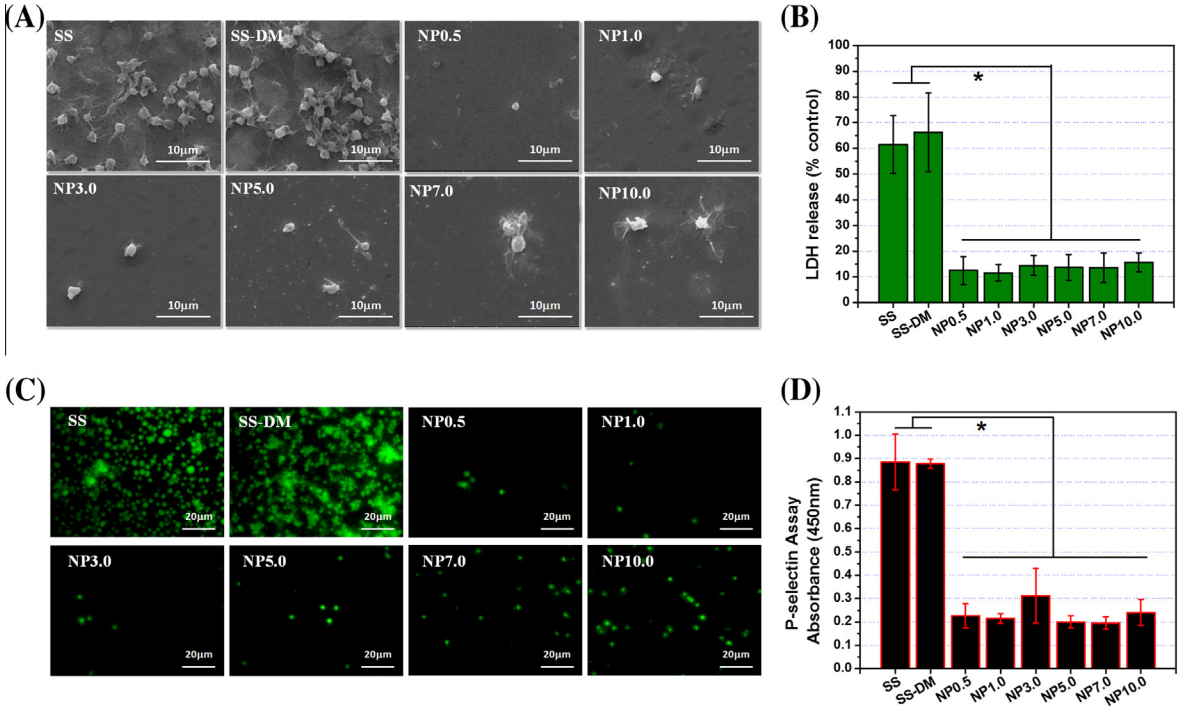

Fig. 7. (A) SEM images of adherent platelets on different sample surfaces; (B) semiquantitative characterization of LDH release; (C) p-selectin immunofluorescence staining of activated platelets on different samples; (D) semiquantitative characterization of p-selectin expression (mean ± SD, $n = 8$, $^{*}P < 0.05$ indicates significant difference compared with SS and SS-DM).

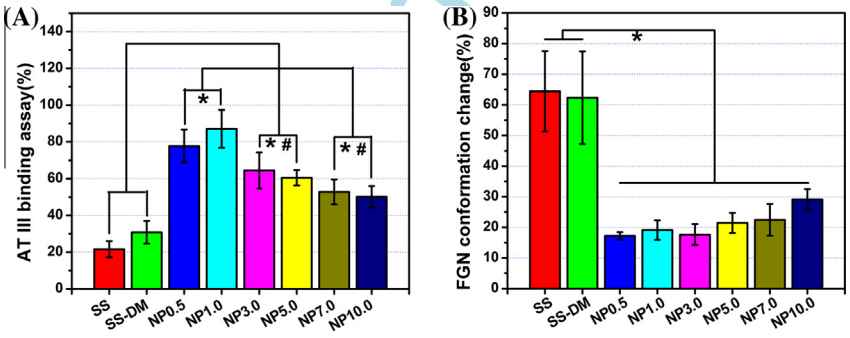

Fig. 8. Relative amount of (A) AT III binding and (B) FGN conformation change on different sample surfaces (mean ± SD, $n = 8$, $^{*}P < 0.05$ indicates significant difference compared with SS and SS-DM, $^{\#}P < 0.05$ indicates significant difference compared with NP0.5 and NP1.0).

enhanced the inactivation rate of AT III to those coagulation proteases by a factor of 2000–4000 [37,38]. To detect the potency of Hep after nanoparticle immobilization, AT III binding was assessed. The conformation change of fibrinogen (FGN) is generally considered to play a critical role in platelet activation and aggregation. Upon interaction with foreign materials, electron transfer between FGN and material surface may occur and subsequently the shielded γ chain becomes accessible. The exposure of the γ chain allowed fibrinogen to bind to the GPIIb/IIIa integrin receptor on the platelet membrane, and caused the adhesion and aggregation of platelets. Therefore, exposed γ chain of FGN on different sample surfaces was determined to further evaluate the anticoagulant property.

As shown in Fig. 8A, the relative binding quantity of AT III was significantly increased ($^{*}P < 0.05$) on the Hep/PLL nanoparticle-immobilized surfaces compared to 316L SS and SS-DM. This demonstrated that the immobilized Hep retained its favorable bioactivity. Furthermore, in comparison with NP0.5 and NP1.0, the AT III binding amount was significantly decreased ($^{\#}P < 0.05$) when the Hep concentration was >3 mg ml^{-1} (Fig. 8A). However, it was obvious that NP10.0 immobilized samples still adsorbed significantly more AT III than bare SS. In addition, compared with SS and SS-DM, the number of exposed γ chains was significantly decreased ($^{*}P < 0.05$) on Hep/PLL nanoparticle-decorated surfaces (Fig. 8B). In addition, there were no significant differences in γ chain quantity among the nanoparticle-immobilized samples; it seems that even a small amount of Hep or negative charges was sufficient to inhibit FGN conformation change.

Above all, these results suggested that Hep/PLL nanoparticle-immobilized surfaces possess favorable AT III binding activity and could significantly prevent FGN conformation change, providing evidence for the anticoagulant behavior observed in platelet adhesion and activation assay.

3.6.3. APTT, PT and TT

Activated partial thromboplastin time (APTT), prothrombin time (PT) and thrombin time (TT) were measured here to further

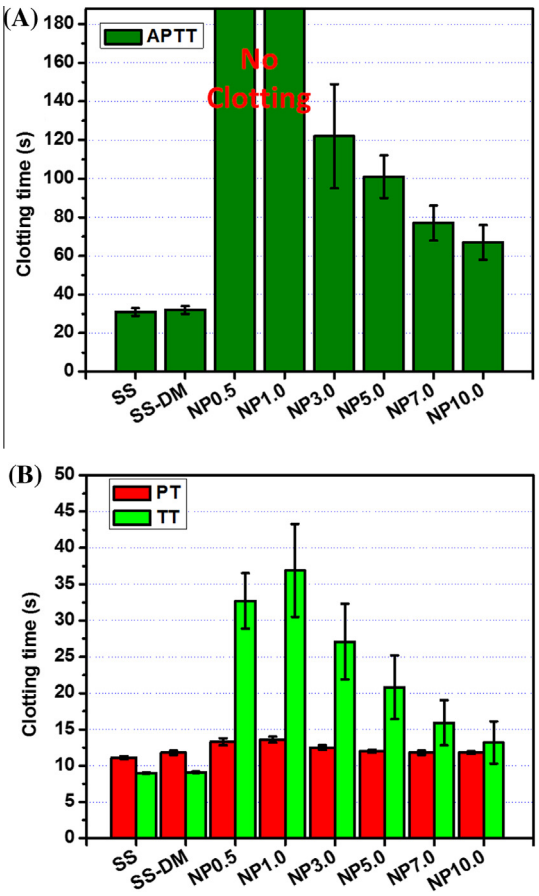

Fig. 9. Clotting time evaluation of different sample surfaces with (A) APTT result and (B) PT and TT result (mean ± SD, $n = 6$).

evaluate the anticoagulation potency of nanoparticle-immobilized samples. APTT and PT are generally considered as performance indicators measuring the efficacy of intrinsic and extrinsic coagulation pathways, respectively, and TT is always used to determine the activity of fibrinolytic systems. APTT is highly sensitive to Hep due to the blocking effect of Hep on the clotting factors IXa, Xa and IIa. Hep–AT III complex is generally considered as the most active inhibitor to clotting factor IIa and XIa, directly influencing the PT value. TT assay was performed to evaluate the effect of nanoparticles on inhibiting thrombin-mediated fibrin formation.

As shown in Fig. 9A, the APTT values of plasma after incubation with Hep/PLL nanoparticle-immobilized surfaces was significantly prolonged compared to SS and SS-DM, and there was no coagulation for NP0.5 and NP1.0 immobilized samples. With increasing Hep concentration, the APTT value presented a falling trend. This result further proved the decrease in Hep density, compactness of particles and reduced Hep release. Although the Hep density of NP10.0 was the lowest among the nanoparticle-immobilized samples, the APTT mean value prolonged by approximately 35 s in comparison with 316L SS, which indicated a significant improvement in the anticoagulant property. However, the effect of Hep/PLL nanoparticles on the PT value appeared quite weak compared to APTT, with only ~1.5–1.8 s prolongation on NP0.5 and NP1.0 immobilized samples and almost no changes on NP7.0 and NP10.0 (Fig. 9B). This may be partly due to the sensitivity of Hep to factor IXa being higher, though the exact mechanisms remain to be resolved. As shown in Fig. 9B, the TT value was extended to ~23.7–27.9 s on NP0.5 and NP1.0 immobilized sample surfaces, and ~4 s on NP10.0, which indicated that Hep/PLL nanoparticle-immobilized surfaces exert a favorable effect on preventing fibrin-induced platelet adhesion.

3.7. EPC, EC and SMC cellular compatibility evaluation

3.7.1. EPC, EC and SMC proliferation

As shown in Fig. S2A, bone marrow stromal cells (BMSCs) always presented a fusiform or multiple branch morphology. Under the stimulation of VEGF-containing media, bone marrow-derived EPCs could be separated with BMSCs by their typical cobblestone-like morphology (Fig. S2A and B) and the specific expression of CD34 (Fig. S2C) after 14 days of culture. SMCs were also easily identified by the long spindle shape and specific expression of α-actin (Fig. S2A and B). Although the spreading area of EPCs was significant larger than ECs (Fig. S2B), it seems hard to identify the EPCs and ECs by cell-surface markers only (Fig. S2C). CCK-8 results showed that the proliferation activity of EPCs was significantly higher ($^{*}P < 0.05$) than that of ECs (Fig. S2D); this may be another sign to distinguish EPCs from ECs. Identified EPCs, ECs and SMCs were seeded on Hep/PLL nanoparticle-immobilized surfaces to evaluate the influence of Hep and amine density on the activity of vascular cells. Immunofluorescence staining was used to identify the types and detect the morphologies of adherent cells, and a CCK-8 assay was performed to measure the cell proliferation.

As a result, after 3 days of culture, the numbers of EPCs adhering on NP0.5 and NP1.0 immobilized sample surfaces were significantly decreased compared with 316L SS and SS-DM, and the cells presented a round shape (Fig. 10A1), which suggested serious cytotoxicity. With the continuously increasing Hep concentration, the number of adherent EPCs gradually improved and was comparable to 316L SS on NP3.0 immobilized samples. When the Hep concentration exceeded 5.0 mg ml^{-1}, the EPC growth density obviously increased and cells exhibited typical cobblestone-shape morphology (Fig. 10A1). The CCK-8 results further proved that the proliferation activity of EPCs on NP3.0 and NP5.0 immobilized surfaces was slightly increased compared with SS and SS-DM, and significant higher ($^{*}P < 0.05$, $^{\#}P < 0.05$) on NP7.0 and NP10.0 immobilized surfaces (Fig. 10A2).

EC proliferation showed a tendency similar to that of EPCs; however, with identical seeding density, the EC growth density appeared lower than that of EPCs (Fig. 10B1), which may arise mainly from differences in the proliferation capacity between EPCs and ECs. In addition, according to the CCK-8 result (Fig. 10B2), the proliferation activity of ECs was still limited on the NP3.0 and NP5.0 immobilized sample surfaces; this was in contrast to EPCs. However, on NP7.0 and NP10.0 immobilized surfaces, which presented low Hep and amine density, the CCK-8 value was significantly increased compared with the other groups ($^{*}P < 0.05$, $^{\#}P < 0.05$, $\Delta P < 0.05$) (Fig. 10B2).

For SMC culture, it was interesting to note that both high and low Hep density could inhibit SMC adhesion and proliferation (Fig. 10C1). Compared with the elongated spindle morphology on the 316L SS and SS-DM sample surfaces, SMCs presented apoptotic shrinkage morphology on NP0.5 and NP1.0 modified surfaces, and with increasing Hep concentration, slight spreading could be observed (Fig. 10C1). When the Hep concentration reached 7.0 mg ml^{-1}, it seems that the adhered cells presented normal spindle morphology, but the density remained significantly decreased (Fig. 10C1). The CCK-8 result was consistent with the microscopy observation: as shown in Fig. 10C2, DM coating could inhibit the SMC proliferation to some degree, but after immobilization of various nanoparticles, the SMC growth activity was decreased to almost the minimum level ($^{*}P < 0.05$). However, the CCK-8 value on NP7.0 and NP10.0 immobilized surfaces was significant higher than on NP0.5 and NP1.0 immobilized surfaces ($^{\#}P < 0.05$). The SMC proliferation rate result (Fig. S3)

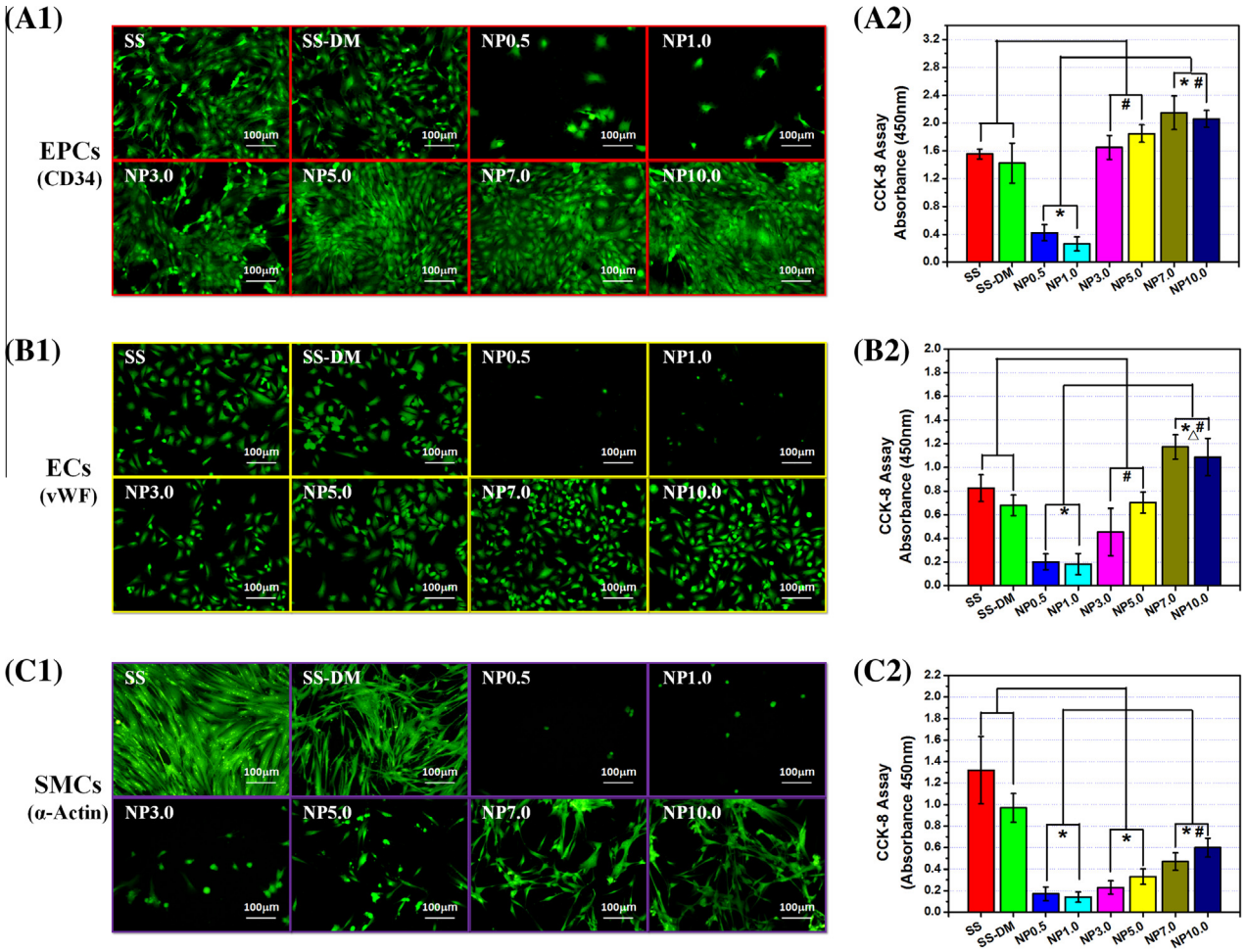

Fig. 10. Immunofluorescence staining of specific cell surface antigens of (A1) CD34 for EPCs (B1) vWF for ECs and (C1) α-actin for SMCs after 3 days of culture; (A2–C2) refers to the related CCK-8 results (mean ± SD, $n = 8$, $^{*}P < 0.05$ indicates significant difference compared with SS and SS-DM, $^{\#}P < 0.05$ indicates significant difference compared with NP0.5 and NP1.0, $\Delta P < 0.05$ indicates significant difference compared with NP3.0 and NP5.0).

demonstrated that the proliferation activity of SMCs on NP0.5 and NP7.0 immobilized surface was significantly inhibited ($^{*}P < 0.05$). Furthermore, although the NP10.0 immobilized surface presented comparable SMC proliferation kinetics in compared with Ti-DM, it was significantly lower ($^{\#}P < 0.05$) than 316L SS (Fig. S3B).

3.7.2. NO release of ECs and EPCs

NO, the endothelium-derived relaxing factor, played a key role in the maintenance of vascular homeostasis by inhibiting excessive vascular SMC proliferation, platelet aggregation and leukocyte adhesion [39]. In addition, the mobilization and differentiation of EPCs are also mediated by NO [40]. This work investigated the influence of Hep and amine density on the NO release activity of ECs and EPCs.

In comparison with SS and SS-DM, the NO release of both ECs and EPCs was obviously decreased on NP0.5 and NP1.0 immobilized surfaces ($^{*}P < 0.05$) (Fig. 11), which presented high Hep and amine density. When the Hep concentration increased from 1.0 to 5.0 mg ml^{-1}, the NO release level showed a rapidly and gently rising tendency for EPCs and ECs, respectively (Fig. 11). The NO biosynthesis activity of EPCs and ECs which adhered on NP7.0 and NP10.0 immobilized surfaces was significantly improved compared to SS and SS-DM ($^{*}P < 0.05$), as well as compared to NP0.5 and NP1.0 ($^{\#}P < 0.05$) (Fig. 11). In addition, it was interesting to

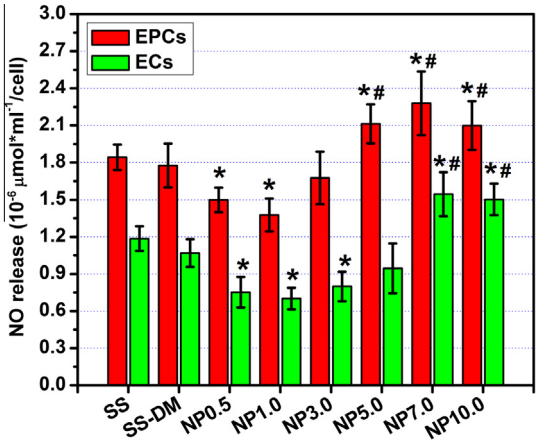

Fig. 11. 12 h cumulative NO release level of EPCs and ECs that adhered on different sample surfaces (mean ± SD, $n = 8$, $^{*}P < 0.05$ indicates significant difference compared with SS and SS-DM, $^{\#}P < 0.05$ means significant difference compared with NP0.5 and NP1.0).

note that the NO release activity of EPCs was significant higher ($P < 0.05$) than that of ECs, which may be partly related to the different proliferation capacity of EPCs and ECs.

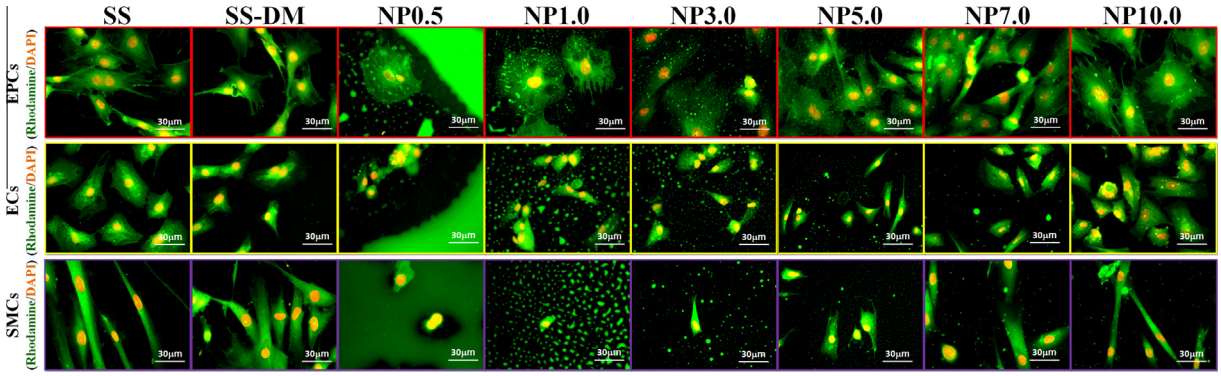

Fig. 12. Rhodamine and DAPI double-fluorescence staining to investigate the interactions between nanoparticles and vascular cells.

3.7.3. Fluorescence staining of cells and nanoparticles

Rhodamine is commonly used as a cationic fluorescent dye for cell staining. However, it was found in this work that Hep/PLL nanoparticles could also be stained by rhodamine123 after glutaraldehyde fixing, which may due to the electrostatic interaction with Hep and the crosslinking effect of glutaraldehyde. DAPI is a fluorescent dye that binds strongly to A-T-rich regions in DNA and is commonly used for cell nucleus staining. Making use of these characteristics, rhodamine and DAPI double fluorescence staining was used to investigate the interactions between nanoparticles and cells.

As shown in Fig. 12, consistent with the AFM results (Fig. 5), NP0.5 immobilized on the surfaces mainly as a confluent film, with cells adherent on the free interspaces of the film; they presented a round (EPCs) or a pyknotic shape (ECs, SMCs). An incipient particle structure was formed on NP1.0 immobilized surface and the three types of cells exhibited round morphology when grown above the particles (Fig. 12); however, the projected area of EPCs was significantly higher than that of ECs and SMCs, which indicated better growth activity of EPCs. For NP3.0, the particle was uniformly distributed on the sample surfaces and the adherent EPCs presented favorable growth morphology, though the spreading of ECs and SMCs remained suppressed (Fig. 12). At increased Hep concentrations, the particle density gradually decreased and the EPCs acquired an elongated morphology; meanwhile, the spreading area of ECs was also increased when the Hep concentration reached 7.0 mg ml^{-1}. However, the SMCs continue to morphologically show an unhealthy state until the lowest Hep density surface of NP10.0 (Fig. 12).

4. Discussion

Biofunctional surface modifications of coronary artery stents using specific biomolecules have been become a new research hotspot. The CD34 antibody-coated EPC capture stent was one of the first platforms to be subject to clinical assessment; this stent was demonstrated to be safe and feasible for the treatment, but a higher rate of major adverse cardiac events was presented after 6 months compared with bare 316L SS stent, as well as an increased rate of thrombosis [41]. Nowadays, it remains problematic to construct a functional environment on the surface of a material for selective inhibition of neointimal hyperplasia and thrombosis formation, but promotion of endothelialization.

One of the most important limitations is the right combination of functional biomolecules on a surface, while maintaining bioactivity, sufficient quantity and durability. Although numerous approaches have been reported, the conjugation of biofunctional molecules to an inorganic biomaterial with favorable bioactivity and stability continues to be problematic. The development of polydopamine coatings provides a potential way to solve this shortcoming. Lee et al. [42] demonstrated that the dopamine possesses strong non-specific affinity to various substrates and tends to form a compact coating on surfaces via self-polymerization; moreover, dopamine coating has a specific reactivity for biomolecules containing sulfhydryl or amine groups [28,43], which greatly facilitates the linkage of numerous biomolecules to the surface of inorganic materials. Meanwhile, in our previous study, dopamine was found to inhibit SMC proliferation [27], which indicated favorable suppression of intimal hyperplasia. However, poor blood compatibility prevented the potential clinical application of dopamine, and anti-thrombogenic modifications are needed.

Heparin has been widely used as an anticoagulant and possesses incomparable advantages, such as suppression of intimal hyperplasia, and it has anti-inflammatory properties and promotes endothelium regeneration in some cases. However, Hep does not react with dopamine due to the lack of amine groups; although several studies have successfully conjugated Hep to dopamine via a chemical crosslinking approach [44,45], it appears difficult to maintain the bioactivity of Hep and control the grafting density.

PLL has been commonly used to coat tissue cultureware to promote cell adhesion. As a cationic polyelectrolyte, PLL has frequently been used for gene loading and transfection [46–48]. In this study, the positively charged PLL was found to strongly interact with the negatively charged Hep and form nanoparticles in PBS via intermolecular electrostatic interaction. Although a similar concept has been reported by Park et al. [29], the nanoparticle preparation approach and experiment system of this study were significantly different. The presence of PLL introduced abundant amine groups to the nanoparticles, which contribute to the covalent binding of the nanoparticles to the dopamine-coated surface via a Schiff base reaction and thereby facilitate surface heparinization.

Shifts of the Hep:PLL concentration ratio caused a significant change in particle size, uniformity and stability, which have been demonstrated by DLS (Fig. 2A). This has a direct influence on the immobilization profile of the particles on the dopamine-coated surfaces. The success of the immobilization of the various nanoparticles on surfaces was monitored by FTIR, XPS and AFM. It appeared that with increasing Hep concentration, the intensity of specific FTIR absorption peaks gradually decreased (Fig. 3A), as well as the sulfur content (Table 2). Meanwhile, the topography of the nanoparticles on the surface changed from a confluent film coating to more uniform particle shape, with a linear decrease in the particle density (Fig. 5). The quantification of Hep and amine groups (Fig. 4A) further proved the above phenomenon and gave reasonable explanations in combination with the results of the zeta potential measurement (Fig. 2A). In brief, with an increase in the Hep concentration, Hep assembles in the particles by interaction

with the exposed amine group and thereby promotes the compactness and stability of nanoparticles (Fig. 2B). The associated decay of exposed amine groups due to the steric hindrance by Hep depresses the efficiency of the reaction between nanoparticles and dopamine coating. Making use of this behavior, surfaces with controlled graded Hep/amine density on a dopamine surface were constructed. To facilitate subsequent discussion, here, different Hep/amine densities were divided into three levels: (1) high level—high Hep and amine density, mainly including NP0.5 and NP1.0; (2) moderate level—moderate Hep and amine density, mainly including NP3.0 and NP5.0; (3) low level—low Hep and amine density, mainly including NP7.0 and NP10.0.

The stability of the different nanoparticles on the dopamine-coated surface directly influenced the subsequent biological function and biocompatibility. In general, for a drug carrier system, an initial burst release is always considered detrimental but hard to avoid, and sometimes may cause adverse effects. For instance, the burst release of Hep may cause a high local drug concentration which increases the risk of bleeding. The release kinetics of the surface-immobilized Hep in the various nanoparticles was investigated in this work. As shown in Fig. 4B, there was a small initial burst release of Hep from each type of immobilized nanoparticle after 1 day of immersion in PBS, followed by a slower controlled release phase. The initial burst release of Hep has been regarded necessary for preventing acute and subacute thrombosis after material implantation [49]. Meanwhile, initial acute inflammatory cell response within 0–3 days after surgery may also be effectively inhibited [50]. In addition, a low dosage of released Hep poses only a low risk for local bleeding. The low initial burst release in this study can be attributed mainly to the tight interaction between Hep and PLL. Related research concerning this behavior can be found in PLL/DNA complex formation, which has similar driving forces as the Hep/PLL nanoparticles. Yamagata et al. [48] suggested that the stability of the PLL–gene complex positively correlates with the PLL chain length; therefore, the low release rate of Hep in this work seemed primarily due to the high molecular weight of the applied PLL in the range of 150–300 kDa. Moreover, with the improvement in nanoparticle stability, the release rate of Hep also significantly decreased (Fig. 4B). The 4 week Hep release kinetics (Fig. 4B) indicates that the Hep/PLL nanoparticle-immobilized surface offers favorable stability for long-term sustained drug delivery. In general, in-stent restenosis usually occurs within weeks to months after stent deployment [51]. The sustained release of Hep therefore promises a beneficial inhibition of excessive SMC migration and proliferation, and thereby suppresses the occurrence of restenosis.

Favorable hemocompatibility is the most basic requirement that a blood-contacting material should meet for clinical use. Although oral antiplatelet therapy could effectively prevent in-stent thrombosis formation, high dosage and long-term usage of anticoagulants may cause drug dependence and serious side effects such as bleeding [52]. The main advantage of cardiovascular materials with anticoagulant surface modification therefore is a significantly reduced local coagulation, which allows reduction of the systemic anticoagulant therapy at a decreased rate of adverse events. This work comprehensively evaluated the hemocompatibility of surfaces with immobilized Hep/PLL nanoparticles. Heparin exhibits its anticoagulant effect mainly by the specific interaction with AT III, which blocks the thrombin-mediated thrombosis formation. Fig. 8 shows that the binding quantity of AT III correlated directly with the Hep density. The subsequent clotting time assay further confirmed this result. For high-level group (NP0.5 and NP1.0), the APTT value indicated non-coagulation and the TT value was extended by ~23.7–27.9 s compared to 316L SS. With the reduction of the Hep density, the APTT value decreased to ~101–122 s in the moderate-level group (NP3.0 and NP5.0) and to ~67–77 s in the low-level group (NP7.0 and NP10.0); the TT value presented a similar trend (Fig. 8A). However, as shown in Fig. 7, although the amount and activation degree of adherent platelets on nanoparticle-immobilized surfaces were greatly decreased in comparison to 316L SS and SS-DM, no significant changes could be observed between the different nanoparticle-grafted samples. Meanwhile, the FGN conformation change also presented a comparable level on all nanoparticle-modified surfaces (Fig. 8B). These results suggested that the immobilized Hep retained excellent anticoagulant activity on the DM-coated surface and a low Hep density was sufficient to obtain favorable hemocompatibility.

After verifying the hemocompatibility of the Hep/PLL nanoparticle-coated surface, the ability to inhibit SMC proliferation without harm to endothelium regeneration became the focus of the analysis. In a drug-eluting stent platform, antiproliferative drugs and endothelialization-promoting biomolecules have been applied together as drug combinations in order to selectively inhibit intimal hyperplasia but accelerate endothelialization [53,54]; however, the clinical performance was equal or worse compared to traditional DES. Besides, some directional drug delivery systems have been presented that allow targeted bidirectional delivery of an antiproliferative agent to the abluminal side and an endothelialization-promoting drug to the luminal side [55]. However, the complex structure appears hard to fabricate and readily fails followed by the expansion of stent. A simple method to resolve these problems was to find a drug with favorable selectivity and specificity for the different vessel cell types; Hep presented as one of the potential candidates. As an anticoagulant, Hep presents multifunctional characteristics incomparable to other anticoagulant drugs, such as anti-inflammatory and anti-restenosis properties. In addition, although Hep has always been suggested as an inhibitor for cell proliferation, the specific binding with various angiogenic growth factors provides the possibility of accelerated endothelialization. In our previous study, we found that a surface with low Hep density was able to inhibit SMC proliferation but promoted EC growth [18]. The present work exploits the structural difference between the prepared nanoparticles to form surfaces with graded Hep densities, to investigate the influence of Hep density on vascular cell behavior, and to screen for a favorable environment that selectively inhibits SMC proliferation but promotes endothelialization. The cell culture tests demonstrated that the proliferation of EPCs, ECs and SMCs were all inhibited in the high-level group (Fig. 10). In addition, rhodamine fluorescence staining result showed that the cells present a condensed morphology after adhesion to the surface, this phenomenon has been commonly seen with the use of high-dose Hep as an antiproliferative reagent and indicated a harmful effect of high-dose Hep on cells. Furthermore, some cytotoxicity may also result from the high amine density on the NP0.5 and NP1.0 immobilized surfaces, because in our recent studies, vascular cell growth was inhibited when the amine density introduced by high molecular weight PLL exceeded 25 nmol cm^{-2} (Fig. S4). In the moderate Hep level group, EPCs presented favorable proliferation and spreading morphology on the samples, while the growth of ECs and SMCs remained reduced. Taking PLL into consideration, the amine density on moderate level group was ~7.4–17.2 nmol cm^{-2}, the range that was considered to promote vascular cells adhesion (Fig. S4); hence, it is reasonable to believe that the inhibition effect on EC and SMC proliferation was mainly related to the Hep amount, but the advantage of NP5.0 to EPC growth may be due to the combined action of Hep and amine. ECs adhering on the surfaces of the low Hep level group exhibited increased growth, whereas the proliferation of SMCs remained poor when exposed amine density was below 6 nmol cm^{-2} and apparently had no significant influence on cell adhesion (Fig. S4); this provides evidence demonstrating that the role of the low-level group both in promoting EC adhesion and inhibiting SMC growth was due to the existence of low-density Hep. The different action

of Hep on direct vascular cell behavior is believed to be possibly due to the specific interaction with Hep-binding cytokines that existed in culture medium or were released from cultured cells. Although Hep is known to inhibit cell growth by blocking selectin-mediated cell adhesion, increased activity of endothelium friendly cytokines may enhance EC and EPC proliferation when Hep is available in sufficient amounts. From the above results, it can be concluded that the contact inhibition effect of various vascular cells to Hep differed, decreasing in the order SMCs > ECs > EPCs. Heparin density at the range of ~3–7 μg cm^{-2} was suggested to result in excellent hemocompatibility and protection from SMC hyperplasia, but significantly accelerated endothelialization.

An ideal combination of surface chemistry and biology is necessary for cardiovascular devices to satisfy clinical requirements. Hence, the bioactivity, quantity and durability of immobilized functional molecules are important; however, they also pose major limitations. In this work, Hep was immobilized on a dopamine-coated surface in the form of nanoparticles; the bioactivity of Hep was well retained and the durability of the material proved excellent. The optimum amount of Hep to selectively direct platelet and vascular cell behavior was also screened by biological evaluation of controlled Hep surface concentrations. However, this still appears insufficient to regulate EPC mobilization, migration, homing and differentiation, which are critical in re-endothelialization of cardiovascular devices. Subsequent studies will take advantage of the specific interaction of Hep with numerous growth factors, and specific cytokine-loaded nanoparticles will be prepared to further resolve these shortcomings.

5. Conclusion

A novel and simple approach to biomaterials surface heparinization has been introduced in the present work. The Hep immobilized on a dopamine-coated surface exhibits excellent stability and anticoagulant activity in the form of Hep/PLL nanoparticles. Surfaces with controlled graded Hep densities from 3.5 ± 0.7 to 43.1 ± 5.1 μg cm^{-2} were created by utilizing the structural characteristic of different nanoparticles. Evaluation of the biological compatibility suggested that a high Hep density above 20 μg cm^{-2} was unsuitable for vascular cell proliferation and endothelium regeneration, while low Hep density up to 3.5 μg cm^{-2} selectively prevented SMC proliferation but accelerated endothelialization. This work has potential application for the design of coronary artery stent surfaces tailored for vascular cell behavior.

Acknowledgments

The authors gratefully acknowledge the assistance from Prof. Yuancong Zhao and Dr. Jialong Chen, and the financial support of Key Basic Research Program (2011CB606204), National Natural Science Foundation of China (No. 31170916#), and the Fundamental Research Funds for the Central Universities (No. SWJTU11ZT11).

Appendix A. Supplementary data

Supplementary data associated with this article can be found, in the online version, at http://dx.doi.org/10.1016/j.actbio.2013.12.013.

Appendix B. Figures with essential color discrimination

Certain figures in this article, particularly Figs. 1–12, are difficult to interpret in black and white. The full color images can be found in the on-line version, at http://dx.doi.org/10.1016/j.actbio.2013.12.013.

References

[1] Windecker S, Meier B. Late coronary stent thrombosis. Circulation 2007;116(17):1952–65.
[2] Byrne RA, Mehilli J, Iijima R. A polymer-free dual drug-eluting stent in patients with coronary artery disease: a randomized trial vs. polymer-based drug-eluting stents. Eur Heart J 2009;30(8):923–31.
[3] Li GC, Yang P, Qin W, Maitz MF, Zhou S, Huang N. The effect of coimmobilizing heparin and fibronectin on titanium on hemocompatibility and endothelialization. Biomaterials 2011;32:4691–703.
[4] Yang ZL, Wang J, Luo RF, Maitz MF, Jing FJ, Sun H, et al. The covalent immobilization of heparin to pulsed-plasma polymeric allylamine films on 316L stainless steel and the resulting effects on hemocompatibility. Biomaterials 2010;31(8):2072–83.
[5] Guo FR, Cheng XY, Wang SF, Zhao YC, Gao Y, Cai HB. Heparin-immobilized polymers as non-inflammatory and non-thrombogenic coating materials for arsenic trioxide eluting stents. Acta biomater 2010;6(2):534–46.
[6] Bjork I, Lindahl U. Mechanism of the anticoagulant action of heparin. Mol Cell Biochem 1982;48(3):161–82.
[7] Cindhuchao N, Quinn DA, Garg HG, Hales CA. Heparin inhibits SMC growth in the presence of human and fetal bovine serum. Biochem Biophys Res Commun 2003;302(1):84–8.
[8] Hoshi RA, Van Lith R, Jen MC, Allen JB, Lapidos KA, Ameer G. The blood and vascular cell compatibility of heparin-modified ePTFE vascular grafts. Biomaterials 2013;34(1):30–41.
[9] Guyton JR, Rosenberg RD, Clowes AW, Karnovsky MJ. Inhibition of rat arterial smooth muscle cell proliferation by heparin. In vivo studies with anticoagulant and nonanticoagulant heparin. Circ Res 1980;46(5):625–34.
[10] Ahn YK, Jeong MH, Kim JW, Kim SH, Cho JH, Cho JG, et al. Preventive effects of the heparin-coated stent on restenosis in the porcine model. Catheter Cardiovasc Interv 1999;48(3):324–30.
[11] Serruys PW, van Hout B, Bonnier H, Legrand V, Garcia E, Macaya C, et al. Randomised comparison of implantation of heparin-coated stents with balloon angioplasty in selected patients with coronary artery disease (Benestent II). Lancet 1998;352(9129):673–81.
[12] Boyle JP, Smart RH, Shirey JK. Heparin in the treatment of chronic obstructive bronchopulmonary disease. Am J Cardiol 1964;14:25–8.
[13] Fine NL, Shim C, Williams MH. Objective evaluation of heparin in the treatment of asthma. Am Rev Respir Dis 1968;98:886–7.
[14] Conrad HE. Heparin-binding proteins. New York, London: Academic Press; 1998.
[15] Yu J, Wang AJ, Tang ZY, Henry J, Lee BLP, Zhu YQ, et al. The effect of stromal cell-derived factor-1α/heparin coating of biodegradable vascular grafts on the recruitment of both endothelial and smooth muscle progenitor cells for accelerated regeneration. Biomaterials 2012;33(32):8062–74.
[16] Cariou R, Harousseau JL, Tobelem G. Inhibition of human endothelial cell proliferation by heparin and steroids. Cell Biol Int Rep 1988;12(12):1037–47.
[17] Khorana AA, Sahni A, Altland OD, Francis CW. Heparin inhibition of endothelial cell proliferation and organization is dependent on molecular weight. Arterioscler Thromb Vasc Biol 2003;23(11):2110–5.
[18] Yang ZL, Tu QF, Wang J, Huang N. The role of heparin binding surfaces in the direction of endothelial and smooth muscle cell fate and re-endothelialization. Biomaterials 2012;33(28):6615–25.
[19] Sakiyama-Elbert SE. Incorporation of heparin into biomaterials. Acta Biomater 2013;10(4):1581–7.
[20] Wang XH, Li DP, Wang WJ, Feng QL, Cui FZ, Xu YX, et al. Covalent immobilization of chitosan and heparin on PLGA surface. Int J Biol Macromol 2003;33(1–3):95–100.
[21] Liu S, Liu T, Chen J, Maitz M, Chen C, Huang N. Influence of a layer-by-layer-assembled multilayer of anti-CD34 antibody, vascular endothelial growth factor, and heparin on the endothelialization and anticoagulation of titanium surface. J Biomed Mater Res A 2013;101(4):1144–57.
[22] Lee J, Yoo JJ, Atala A, Lee SJ. Controlled heparin conjugation on electrospun poly(ε-caprolactone)/gelatin fibers for morphology-dependent protein delivery and enhanced cellular affinity. Acta Biomater 2012;8(7):2549–58.
[23] Zhang F, Fath M, Marks R, Linhardt RJ. A highly stable covalent conjugated heparin biochip for heparin-protein interaction studies. Anal Biochem 2002;304(2):271–3.
[24] Chen H, Chen Y, Sheardown H, Brook MA. Immobilization of heparin on a silicone surface through a heterobifunctional PEG spacer. Biomaterials 2005;26:7418e24.
[25] Tsai WB, Chen WT, Chien HW, Kuo WH, Wang MJ. Poly(dopamine) coating of scaffolds for articular cartilage tissue engineering. Acta Biomater 2011;7(12):4187–94.
[26] Joddar B, Albayrak A, Kang J, Nishihara M, Abe H, Ito Y. Sustained delivery of siRNA from dopamine-coated stainless steel surfaces. Acta Biomater 2013;9(5):6753–61.
[27] Yang ZL, Tu QF, Zhu Y, Luo RF, Li X, Xie YC, et al. Mussel-inspired coating of polydopamine directs endothelial and smooth muscle cell fate for re-endothelialization of vascular devices. Adv Healthc Mater 2012;1(5):548–59.
[28] Weng Y, Song Q, Zhou Y, Zhang L, Wang J, Chen J, et al. Immobilization of selenocystamine on TiO_2 surfaces for in situ catalytic generation of nitric oxide

and potential application in intravascular stents. Biomaterials 2011;32(5):1253–63.
[29] Park JS, Park K, Woo DG, Yang HN, Chung HM, Park KH. Triple constructs consisting of nanoparticles and microspheres for bone-marrow-derived stromal-cell-delivery microscaffolds. Small 2008;4(11):1950–5.
[30] Merdan T, Kopecek J, Kissel T. Prospects for cationic polymers in gene and oligonucleotide therapy against cancer. Adv Drug Deliv Rev 2002;54(5):715–58.
[31] Smith PK, Mallia AK, Hermanson GT. Colorimetric method for the assay of heparin content in immobilized heparin preparations. Anal Biochem 1980;109(2):466–73.
[32] Hamerli P, Weigel T, Groth T, Paul D. Surface properties of and cell adhesion onto allylamine–plasma-coated polyethylenterephtalat membranes. Biomaterials 2003;24(22):3989–99.
[33] Li QL, Huang N, Chen C, Chen JL, Xiong KQ, Chen JY, et al. Oriented immobilization of anti-CD34 antibody on titanium surface for self-endothelialization induction. J Biomed Mater Res A 2010;94:1283–93.
[34] Hanaor D, Michelazzi M, Leonelli C, Sorrell CC. The effects of carboxylic acids on the aqueous dispersion and electrophoretic deposition of ZrO_2. J Eur Ceram Soc 2012;32(1):235–44.
[35] Monchaux E, Vermette P. Effects of surface properties and bioactivation of biomaterials on endothelial cells. Front Biosci (Schol Ed) 2010;2:239–55.
[36] Hattori R, Hamilton KK, Fugate RD, McEver RP, Sims PJ. Stimulated secretion of endothelial von Willebrand factor is accompanied by rapid redistribution to the cell surface of the intracellular granule membrane protein GMP-140. J Biol Chem 1989;264(14):7768–71.
[37] Olson ST, Bjork I. Predominant contribution of surface approximation to the mechanism of heparin acceleration of the antithrombin-thrombin reaction. Elucidation from salt concentration effects. J Biol Chem 1991;26:6353–64.
[38] Olson ST, Bjork I, Sheffer R, Craig PA, Shore JD, Choay J. Role of the antithrombin-binding pentasaccharide in heparin acceleration of antithrombin-proteinase reactions. Resolution of the antithrombin conformational change contribution to heparin rate enhancement. J Biol Chem 1992;267:12528–38.
[39] Moncada S. Nitric oxide in the vasculature: physiology and pathophysiology. Ann N Y Acad Sci 1997;811:60–7 (discussion: 67–9).
[40] Thum T, Tsikas D, Stein S, Schultheiss M, Eigenthaler M, Anker SD, et al. Suppression of endothelial progenitor cells in human coronary artery disease by the endogenous nitric oxide synthase inhibitor asymmetric dimethylarginine. J Am Coll Cardiol 2005;46:1693–701.
[41] Červinka P, Bystroň M, Špaček R, Kvašňák M, Jakabčin J. Randomized Comparison of Genous Stent Versus Chromium-Cobalt stent for Treatment of ST-Elevation Myocardial Infarction. 6-month Clinical, Angiographic and IVUS Follow-up. GENIUS-STEMI trial. Presented at the American College of Cardiology Annual Scientific Session 2009.
[42] Lee H, Dellatore SM, Miller WM, Messersmith PB. Mussel-inspired surface chemistry for multifunctional coatings. Science 2007;318:426–30.
[43] Lee H, Rho J, Messersmith PB. Facile conjugation of biomolecules onto surfaces via Mussel adhesive protein inspired coatings. Adv Mater 2009;21(4):431–4.
[44] Joung YK, You SS, Park KM, Go DH, Park KD. In situ forming, metal-adhesive heparin hydrogel surfaces for blood-compatible coating. Colloids Surf B Biointerfaces 2012;99:102–7.
[45] Jung YS, Jeong JH, Yook S, Im BH, Seo J, Hong SW, et al. Surface modification of pancreatic islets using heparin-DOPA conjugate and anti-CD154 mAb for the prolonged survival of intrahepatic transplanted islets in a xenograft model. Biomaterials 2012;33(1):295–303.
[46] Dai J, Zou S, Pei Y, Cheng D, Ai H, Shuai X. Polyethylenimine-grafted copolymer of poly(l-lysine) and poly(ethylene glycol) for gene delivery. Biomaterials 2011;32(6):1694–705.
[47] Zhou D, Li C, Hu Y, Zhou H, Chen J, Zhang Z, et al. Glycopolymer modification on physicochemical and biological properties of poly(L-lysine) for gene delivery. Int J Biol Macromol 2012;50(4):965–73.
[48] Yamagata M, Kawano T, Shiba K, Mori T, Katayama Y, Niidome T. Structural advantage of dendritic poly(L-lysine) for gene delivery into cells. Bioorg Med Chem 2007;15(1):526–32.
[49] Lakshmi TS, Shanmugasundaram N, Shanmuganathan S, Karthikeyan K, Meenakshi J, Babu M. Controlled release of 2, 3 desulfated heparin exerts its anti-inflammatory activity by effectively inhibiting E-selectin. J Biomed Mater Res A 2010;95(1):118–28.
[50] Gomes WJ, Buffolo E. Coronary stenting and inflammation: implications for further surgical and medical treatment. Ann Thorac Surg 2006;81(5):1918–25.
[51] Haery C, Sachar R, Ellis SG. Drug-eluting stents: the beginning of the end of restenosis? Cleve Clin J Med 2004;71(10):815–24.
[52] Rossini R, Baroni M, Musumeci G, Gavazzi A. Oral antiplatelet therapy after drug-eluting stent implantation: adherence and side-effects. J Cardiovasc Med (Hagerstown) 2013;14(2):81–90.
[53] Verheye S, Agostoni P, Dawkins KD, Dens J, Rutsch W, Carrie D, et al. The GENESIS (randomized, multicenter study of the pimecrolimus-eluting and pimecrolimus/paclitaxel-eluting coronary stent system in patients with de novo lesions of the native coronary arteries) trial. JACC Cardiovasc Interv 2009;2(3):205–14.
[54] Adriaenssens T, Mehilli J, Wessely R, Ndrepepa G, Seyfarth M, Wieczorek A, et al. Does addition of estradiol improve the efficacy of a rapamycin-eluting stent? Results of the ISAR-PEACE randomized trial. J Am Coll Cardiol 2007;49(12):1265–71.
[55] Wessely R. New drug-eluting stent concepts. Nat Rev Cardiol 2010;7(4):194–203.